Electronic Supplementary Material (ESI) for Physical Chemistry Chemical Physics.

Supplemental Materials

Effect of Ni atomic fraction on active species of graphene growth on Cu-Ni alloy catalysts: a density functional theory study

Erik Bhekti Yutomo, Fatimah Arofiati Noor*, Toto Winata

Physics of Electronic Materials Research Division, Department of Physics, Faculty of Mathematics and Natural Sciences, Institut Teknologi Bandung, Jalan Ganesa no. 10 Bandung 40132, Indonesia.

*Corresponding author: fatimah@itb.ac.id

S1. Structural parameters of the carbon source species

Table S1 compares the optimized C-H bond lengths, d_{C-H}, of the radical species CH_n (n=1,2,3) with the previous experimental and computational studies.

Table S1. Comparison of the optimized C-H bond lengths, d_{C-H}, of the radical species CH_n (n=1,2,3)

Radical species	d_{C-H}		
	This study	Previous experimental study [1]	Previous computational study [2]
CH_3	1.087	-	-
CH_2	1.086	1.085	1.084
CH	1.137	1.120	1.132

S2. The effect of Ni atoms on the Cu-Ni alloy catalyst.

Two possible structures for the Cu-Ni-1 and Cu-Ni-2 catalysts are shown in Fig. S1. The calculated doping formation energy is also included.

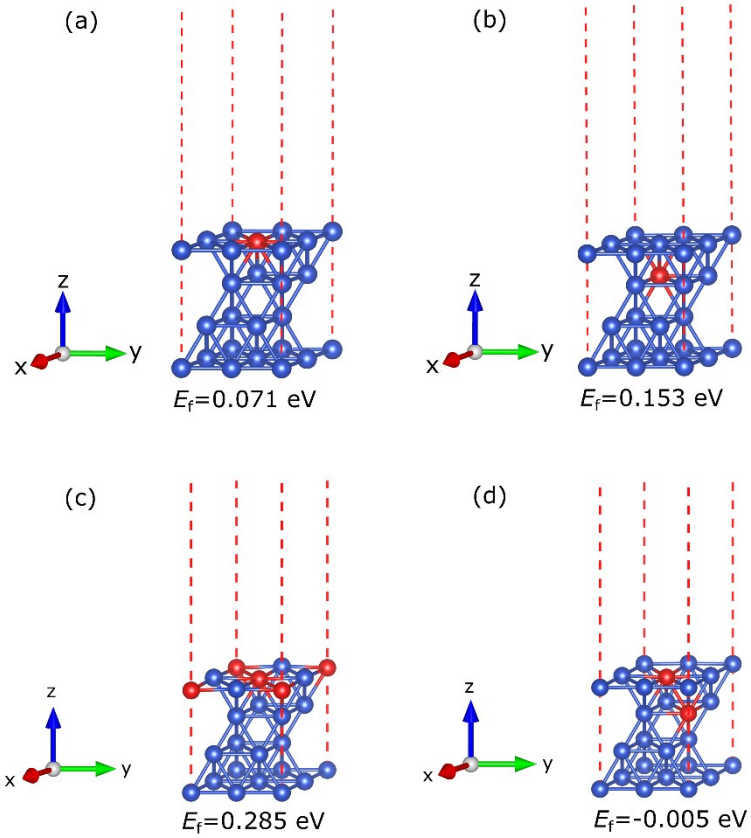

Fig. S1. Comparison of the doped formation energy of the possible configurations of the (a,b) Cu-Ni-1, and (c,d) Cu-Ni-2 catalysts.

The total density of states (TDOS) and the projected density of states (PDOS) of the d-orbitals of Cu-Ni-2 and Cu-Ni-3 catalysts are shown in Figs. S2(a) and (b), respectively. The PDOS of sub-Ni 3d of Cu-Ni-2 and Cu-Ni-3 catalysts system are presented. Furthermore, the charge density differences of the Cu-Ni-2 and Cu-Ni-3 catalysts are shown in Figs. S2(c) and (d), respectively.

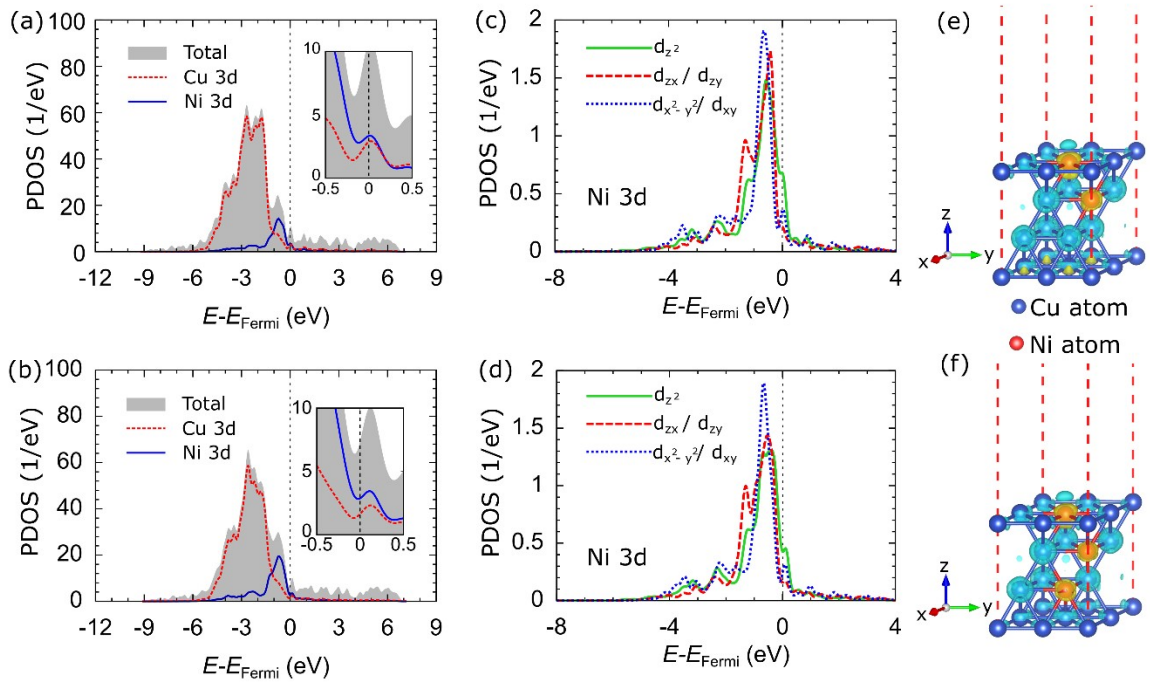

Fig. S2. Total density of states (TDOS) and projected density of states (PDOS) of the d-orbitals of (a) Cu-Ni-2 and (b) Cu-Ni-3 catalysts. The PDOS of sub-Ni 3d of (c) Cu-Ni-2 and (d) Cu-Ni-3 catalysts system are presented. The black dashed line indicates the Fermi level. The charge density difference in (e) Cu-Ni-2 and (f) Cu-Ni-3 catalysts is illustrated by the iso-surface of 0.01 e/Å. Yellow and blue clouds indicate electron accumulation and depletion, respectively.

S3 Adsorption of carbon source species on the catalyst surface

A comparison of the calculated adsorption energies and equilibrium distances of the carbon source species on the Cu catalyst is shown in Table S2.

Table S2. Adsorption energies, E_{ads}, and equilibrium distances, Z_A, of the carbon source species and H_2O on the Cu catalyst surface

carbon source species	Sites	This calculation		Previous study	
		E_{ads} (eV)	Z_A (Å)	E_{ads} (eV)	Z_A (Å)
CH_4	hcp	−0.190	2.715		
	fcc	−0.190	2.729		
	top	−0.163	2.416	−0.169[(a)], −0.160[(c)]	
	bri	−0.177	2.656		
CH_3	hcp	−2.667	2.203	−2.710[(a)], −1.850[(c)]	2.206[(c)]
	fcc	−2.653	2.195	−2.528[(a)], −1.850[(c)]	2.204[(c)]
	top	−2.504	1.994	−2.571[(a)]	1.990[(c)]
	bri	−2.572	2.120		
CH_2	hcp	−4.095	1.989	−4.071[(a)], −3.550[(c)]	1.971[(c)]
	fcc	−4.136	1.987	−4.110[(a)], −3.570[(c)]	1.971[(c)]
	top	−3.252	1.835	−3.294[(a)]	
	bri				
CH	hcp	−5.633	1.904	−5.592[(a)], −5.340[(c)]	1.910[(c)]
	fcc	−5.701	1.904	−5.662[(a)], −5.400[(c)]	1.908[(c)]
	top	−3.878	1.733		
	bri				
C_{surf}	hcp	−6.204	1.832	−6.178[(b)]	1.845[(b)]
	fcc	−6.245	1.838	−6.238[(b)]	1.847[(b)], 1,98[(d)]
	top	−4.272	1.748	−4.281[(b)]	1.750[(b)]
	bri	−6.109	1.806	−6.178[(b)]	1.808[(b)]
H_2O	top	−0.408	2.346	−0.390 [(d)]	

[(a)] is the calculation results of ref. [3], in which the catalyst is modeled with a four-layer (4×4) periodic slab, [(b)] is the calculation results of ref. [4], in which the catalyst is modeled with a five-layer (3×3) periodic slab, [(c)] is the calculation results of ref. [5], in which the catalyst is modeled with a three-layer (3×3) periodic slab, and [(d)] is the experimental result of ref. [6], [(d)] is the calculation results of ref. [7], in which the catalyst is modeled with a five-layer (3×3) periodic slab

The calculated adsorption energies of the carbon source species on the Cu-Ni catalyst surface with various Ni atomic fractions are shown in Table S3.

Table S3. Adsorption energies E_{ads} of the carbon source species and H_2O on the Cu-Ni catalyst surface with various Ni atomic fractions

Cu-Ni-1										
carbon source species	$E_{ads}\ (eV)$									
	$hcp_{3Cu\text{-}Cu}$	$fcc_{3Cu\text{-}Cu}$	$hcp_{2CuNi\text{-}Cu}$	$fcc_{2CuNi\text{-}Cu}$	top_{Cu}	top_{Ni}	bri_{CuCu}	bri_{CuNi}		
CH_3		−1,837		−2,572	−2.068	−2.685	−2.000	−2.422		
CH_2	−3.959	−3.823	−4.490	−4.572		−4.055				
CH	−5.578	−5.565	−6.232	−6.313		−5.034				
C_{surf}	−6.150	−6.354	−7.075	−7.098		−5.742				
H_2O					−0.503					
Cu-Ni-2										
carbon source species	$E_{ads}\ (eV)$									
	$hcp_{3Cu\text{-}Cu}$	$fcc_{3Cu\text{-}Cu}$	$hcp_{2CuNi\text{-}Cu}$	$fcc_{2CuNi\text{-}Cu}$	$hcp_{2CuNi\text{-}Ni}$	top_{Cu}	top_{Ni}	bri_{CuCu}	bri_{CuNi}	
CH_3		−1.946		−2.694		−2.177	−2.626	−2.109	−2.531	
CH_2	−4.028	−3.892	−4.585	−4.640	−4.449		−4.123			
CH	−5.578	−5.579	−6.259	−6.327	−6.150					
Csurf	−6.161	−6.365	−7.113	−7.107	−6.993					
H_2O					−0.503					
Cu-Ni-3										
carbon source species	$E_{ads}\ (eV)$									
	$hcp_{3Cu\text{-}Cu}$	$fcc_{3Cu\text{-}Cu}$	$hcp_{2CuNi\text{-}Cu}$	$fcc_{2CuNi\text{-}Cu}$	$hcp_{2CuNi\text{-}Ni}$	$fcc_{2CuNi\text{-}Ni}$	top_{Cu}	top_{Ni}	bri_{CuCu}	bri_{CuNi}
CH_3		−2.680		−2.708		−2.612	−2.191	−2.667	−2.123	−2.544
CH_2	−4.068	−4.054	−4.585	−4.680	−4.463	−4.612		−4.163		
CH	−5.606	−5.592	−6.272	−6.340	−6.177	−6.272				
C_{surf}	−6.204	−6.190	−7.130	−7.157	−7.034	−7.062				
H_2O					−0.517					

The optimized structures of the adsorbed carbon source species with the lowest adsorption energies on the surfaces of the Cu and Cu-Ni catalysts are shown in Fig. S3.

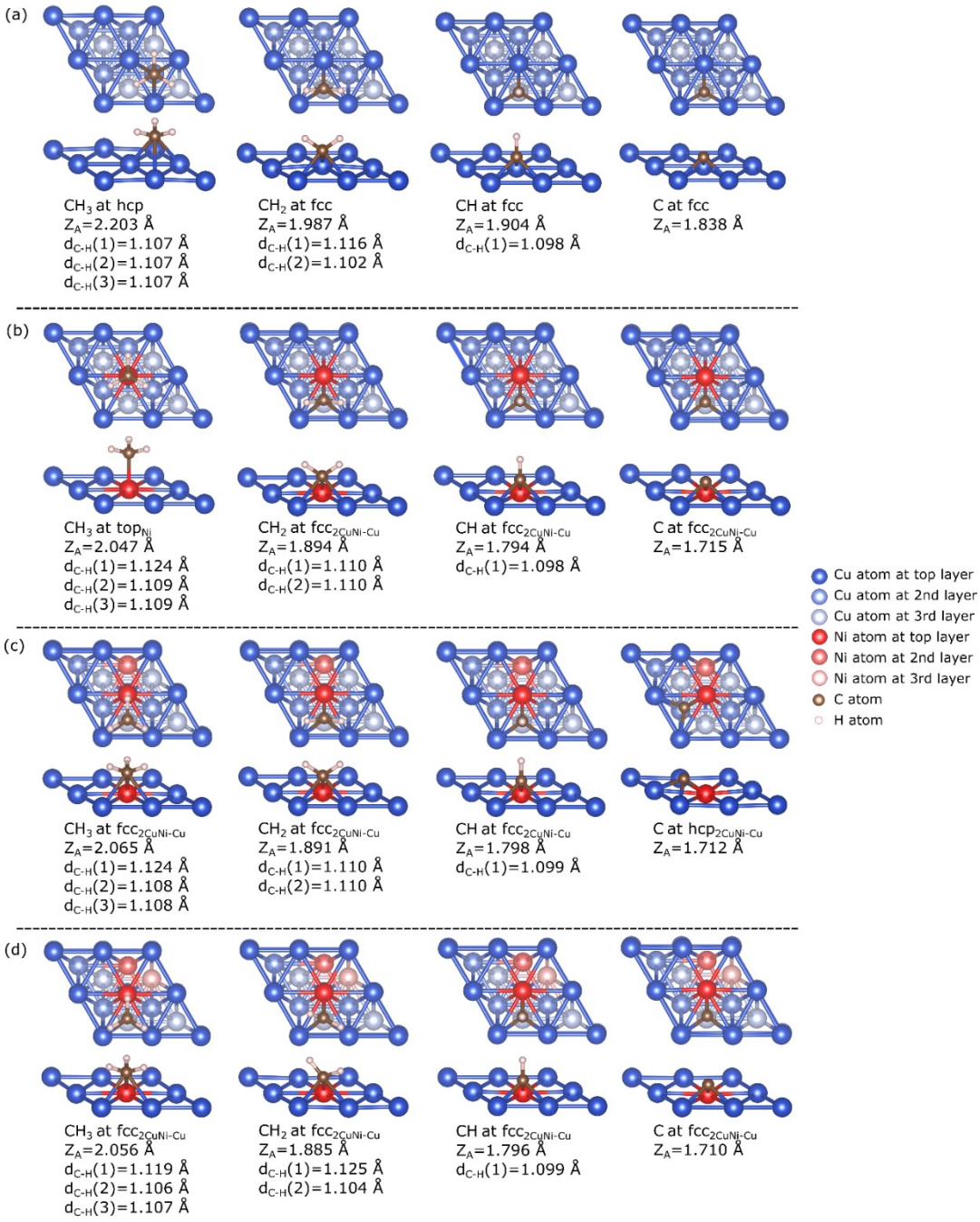

Fig. S3. The optimized structure of the adsorbed carbon source species with the lowest adsorption energy on the surfaces of the (a) Cu, (b) Cu-Ni-1, (c) Cu-Ni-2, and (d) Cu-Ni-3 catalysts surface. The equilibrium distances and optimized C-H bond lengths are also listed.

The charge density differences of carbon source species on the surfaces of the Cu and Cu-Ni catalysts at their respective preferred sites are shown in Fig. S4.

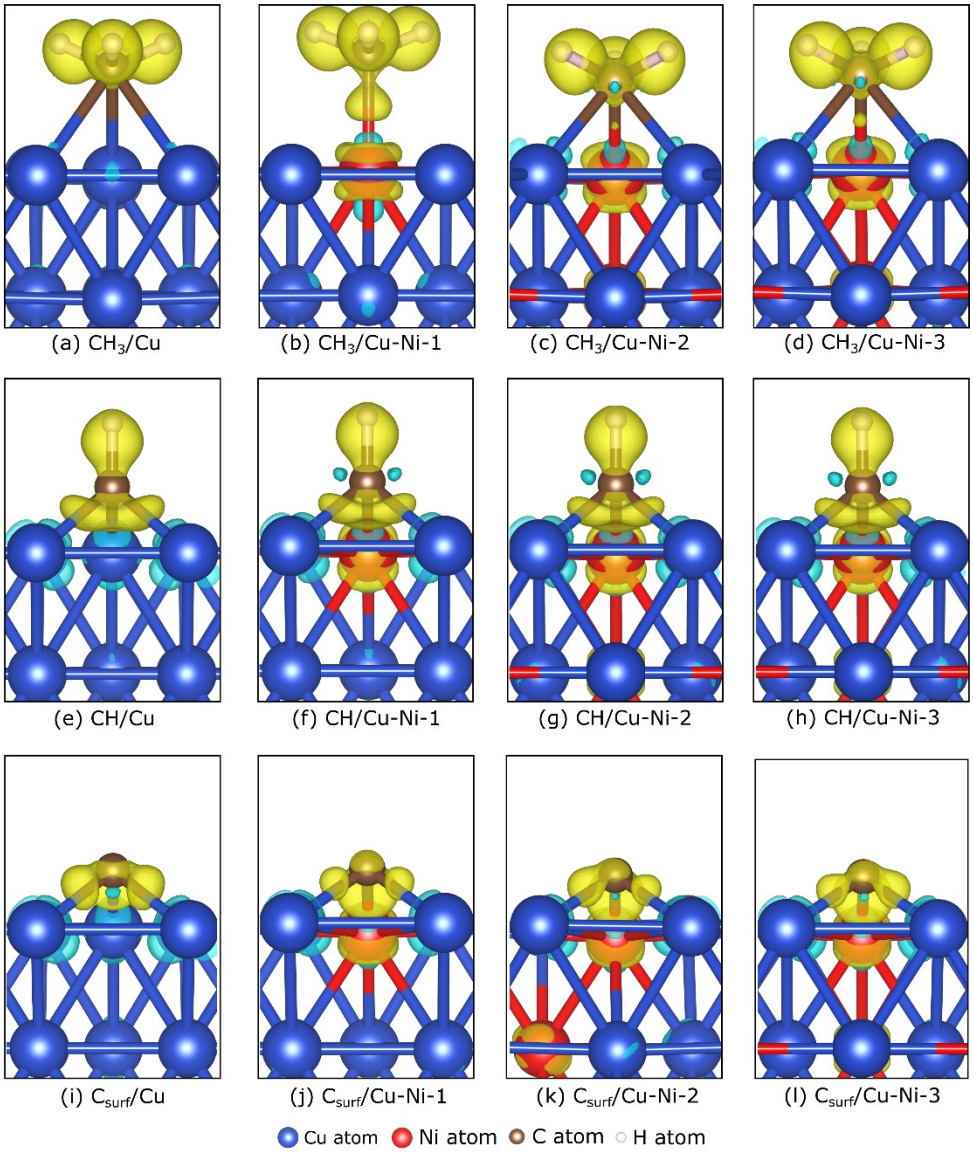

Fig. S4. The charge density differences of (a–d) CH_3, (e–h) CH, and (i–l) C_{surf} on the surfaces of the Cu and Cu-Ni catalysts at their respective preferred sites are illustrated by the 0.015 e/Å iso-surface. Yellow and blue clouds indicate electron accumulation and depletion, respectively.

Fig. S5 shows the local density of states (LDOS) of isolated carbon source species (CH_3, CH, and C) and adsorbed carbon source species on Cu and Cu-Ni catalyst surfaces. The carbon atom in the CH_3 species tends to sp^3 hybridize, forming three σ orbitals (Fig. S5(a)), while the carbon

atom in the CH species tends to sp hybridize, forming two σ orbitals and one π orbital (Fig. S5(b)). The C atom has s and p atomic orbitals (Fig. S5(c)). All adsorption systems show that increasing the fraction of Ni atoms in the alloy catalyst causes the Ni atomic orbitals to shift to a higher energy level, indicating an increase in the d-band center. Moreover, the Ni 3d-orbitals become more delocalized as the atomic fraction of Ni is increased

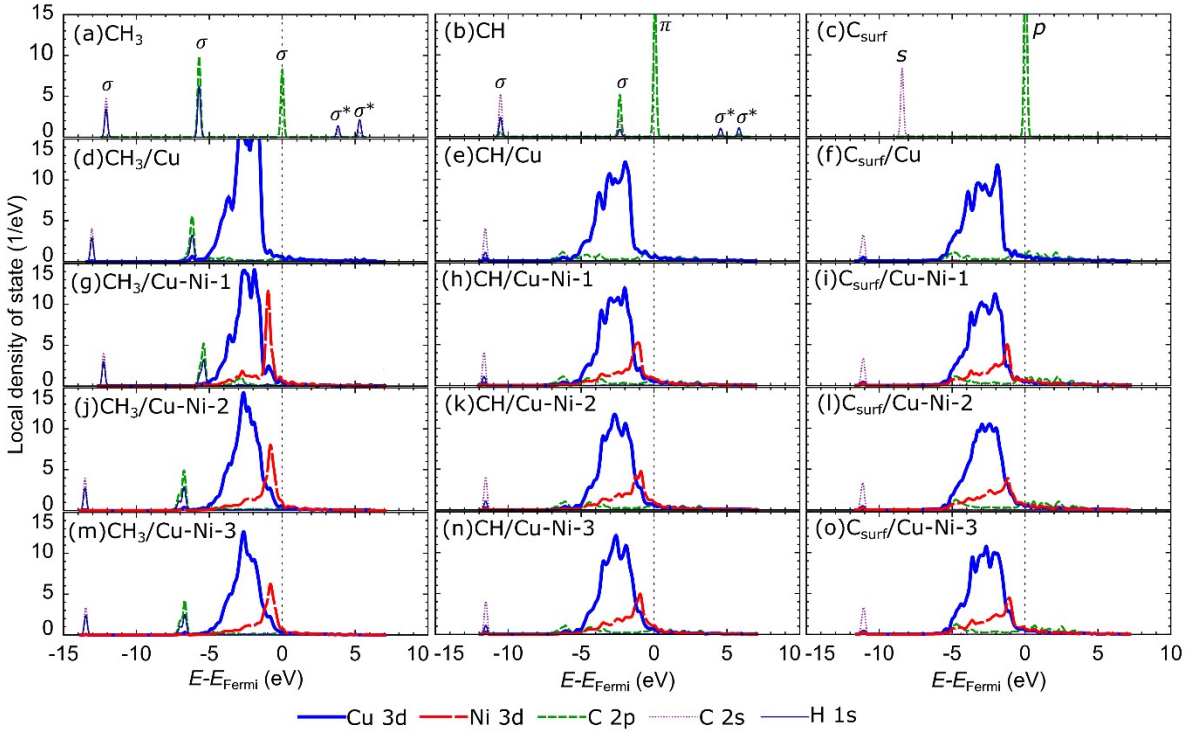

Fig. S5. Local density of states (LDOS) of (a-c) isolated carbon source species, carbon source species on the surface of (d-f) Cu, (g-i) Cu-Ni-1, (j-l) Cu-Ni-2, and (m-o) Cu-Ni-3 catalyst. The d-bands of Cu and Ni are projected to the topmost Cu and Ni atoms, respectively.

S4. Adsorption of a carbon monomer on the catalyst subsurface

The calculated adsorption energies of the carbon monomer species at possible octahedral (*octa*) sites of the Cu and Cu-Ni catalyst subsurfaces are shown in Table S4.

Table S4. The adsorption energies of carbon monomer species at possible octahedral (*octa*) sites of the subsurfaces of the Cu and Cu-Ni catalysts. "N/A" indicates the site is not present on the associated catalyst.

Catalysts	Carbon monomer species	$E_{ads}\ (eV)$			
		$octa_{3Cu\text{-}3Cu}$	$octa_{2CuNi\text{-}3Cu}$	$octa_{3Cu\text{-}2CuNi}$	$Octa_{2CuNi\text{-}2CuNi}$
Cu	$C_{sub\text{-}1}$	−5.837	N/A	N/A	N/A
	$C_{sub\text{-}2}$	−5.660	N/A	N/A	N/A
Cu-Ni-1	$C_{sub\text{-}1}$	−6.517	−7.062	N/A	N/A
	$C_{sub\text{-}2}$	−6.259	N/A	N/A	N/A
Cu-Ni-2	$C_{sub\text{-}1}$	N/A	−6.789	−6.925	−7.334
	$C_{sub\text{-}2}$	−6.245	−6.762	N/A	N/A
Cu-Ni-3	$C_{sub\text{-}1}$	N/A	−6.885	−6.953	−7.415
	$C_{sub\text{-}2}$	N/A	−6.721	−6.708	−7.225

The charge density differences of a carbon monomer on the second subsurfaces of Cu and Cu-Ni catalysts at their respective preferred sites are shown in Fig. S6.

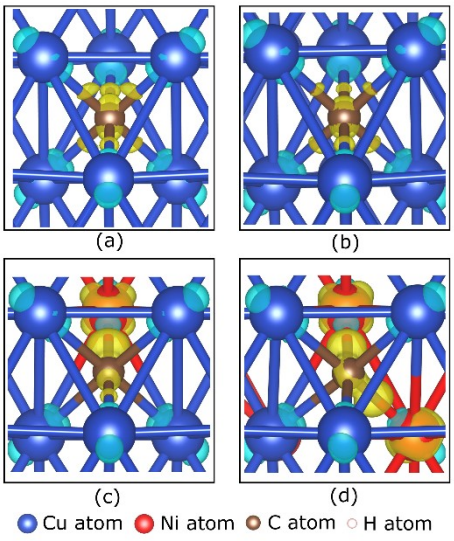

Fig. S6. The charge density differences of a carbon monomer on the second subsurface of (a) Cu, (b) Cu-Ni-1, (c) Cu-Ni-2, and (d) Cu-Ni-3 catalysts at their respective preferred site are illustrated

by the 0.015 e/Å iso-surface. Yellow and blue clouds indicate electron accumulation and depletion, respectively.

Fig. S7 shows the LDOS of an isolated carbon monomer and an adsorbed carbon monomer on the surfaces of Cu and Cu-Ni catalysts.

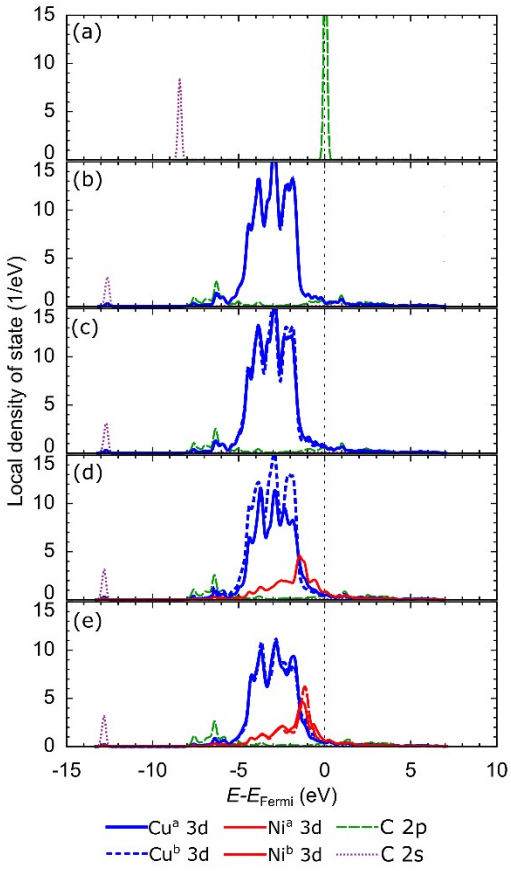

Fig. S7. Local density of states (LDOS) of (a) isolated C, C on the second subsurface of (b) Cu, (c) Cu-Ni-1, (d) Cu-Ni-2, and (e) Cu-Ni-3 catalysts at their preferred sites. The d-bands of Cu and Ni are projected to the Cu and Ni atoms above (Cu^a 3d and Ni^a 3d) and below (Cu^b 3d and Ni^b 3d) the second subsurface site, respectively.

S4. Ab initio thermodynamics analysis

The Gibbs free energy of adsorption (ΔG^{ads}) can be calculated using the following equation [8, 9]:

$$\Delta G^{ads} = E_{total} - E_{cat} + F_{vib} - n_C\mu_C - n_H\mu_H \quad \text{(S1)}$$

where E_{total} is the total energy of the adsorbed carbon source species on the catalyst, E_{cat} is the total energy of the catalyst, F_{vib} is a parameter containing the vibrational contribution of the Gibbs free energy, n_C and n_H are the number of C and H atoms in the carbon source species (CH_3, CH_2, CH, C_{surf}, $C_{sub\text{-}1}$, and $C_{sub\text{-}2}$), respectively, and μ_C and μ_H are the chemical potentials of carbon and hydrogen atoms, respectively. The vibrational free energy (F_{vib}) is formulated according to the following equation [8, 10]:

$$F_{vib} = E^{ZPE} + E^{vib} + TS^{vib} \quad \text{(S2)}$$

where E^{ZPE} is the zero point energy, E^{vib} is the vibrational energy, S^{vib} is the vibrational entropy, and T is the system temperature. These three parameters can be calculated from [8, 10]:

$$E^{ZPE} = \sum_i \frac{\hbar\omega_i}{2} \quad \text{(S3)}$$

$$E^{vib} = \sum_i \frac{\hbar\omega_i}{\exp\left(\frac{\hbar\omega_i}{k_BT}\right) - 1} \quad \text{(S4)}$$

$$S^{vib} = k_B\left[\sum_i \frac{\hbar\omega_i}{k_BT\left\{\exp\left(\frac{\hbar\omega_i}{k_BT}\right) - 1\right\}} - \ln\left\{1 - \exp\left(-\frac{\hbar\omega_i}{k_BT}\right)\right\}\right] \quad \text{(S5)}$$

where $\hbar$ is the reduced Plank constant, k_B is the Boltzmann constant, and ω_i is the vibrational frequency of the carbon source species on the catalyst. The vibrational frequency is obtained by diagonalizing the dynamic matrix, in which only the carbon source species are allowed to move. This approach effectively reduces the calculation time while still considering the effect of the catalyst on the vibrational frequency [11, 12]. The calculated vibrational frequencies of the carbon source species in each catalyst are shown in Table S5. We compare the calculated

vibrational frequency with a previous study [13]. Our results are consistent, so we can use the calculated parameters.

The parameter μ_H depends on the T and the H_2 partial pressure, p_{H_2}, which can be calculated using the following equation [9, 14, 15]:

$$2\mu_H = E_{H_2} - k_B T \ln\left(\frac{g k_B T}{p_{H_2}} \zeta_{trans}\, \zeta_{rot}\, \zeta_{vib}\right) \tag{S6}$$

where g is the degree of degeneration of the electron energy level, and E_{H_2} is the total energy of the H_2 molecule obtained from the DFT calculation (our calculation result is −2.399 Ry (−32.641 eV). ζ_{trans}, ζ_{rot}, and ζ_{vib} are partition functions for the translational, rotational, and vibrational motions, respectively. For the H_2 molecule, a diatomic molecule, we can calculate ζ_{trans}, ζ_{rot}, and ζ_{vib} using the following equations [14, 15]:

$$\zeta_{trans} = \left(\frac{2\pi m k T}{h^2}\right)^{1/2} \tag{S7}$$

$$\zeta_{rot} = \frac{T}{\sigma \Theta_r} \tag{S8}$$

$$\zeta_{vib} = \frac{1}{1 - \exp\left(-\frac{\Theta_v}{T}\right)} \tag{S9}$$

where m is the mass of the H atom, σ is the symmetry factor, and Θ_r and Θ_v are the rotational and vibration temperatures of the H_2 molecule, respectively.

Table S5. The vibrational frequencies of carbon source species on the Cu and Cu-Ni catalysts.

Carbon source species	Catalysts	Vibrational frequency (cm^{-1})	
		This study	Previous study [13]
CH_3	gas	536.469, 1351.445, 1351.292, 3046.904, 3225.353, 3225.853	606.5, 1396.0, 1396.0, 3004.4, 3160.8, 3160.8
CH_2	gas	996.870, 2892.304, 3042.647	963.1, 2805.9, 3190.0
CH	gas	2740.802	2733.1
CH_3	Cu	125.484, 125.484,	

		167.955, 325.559, 527.609, 527.609, 1124.971, 1345.361, 1345.361, 2918.810, 2993.108, 2993.109	
CH_2	Cu	149.468, 299.808, 382.032, 388.073, 524.120, 645.050, 1272.822, 2900.294, 2942.063	
CH	Cu	470.932, 470.932, 610.292, 651.950, 651.950, 3067.130	
C_{surf}	Cu	554.756, 554.756, 564.971	
C_{sub-1}	Cu	609.785, 611.517, 611.517	
C_{sub-2}	Cu	593.204, 593.204, 663.872	
CH_3	Cu-Ni-1	223.779, 223.779, 243.720, 494.431, 594.856, 594.856, 1111.215, 1347.689, 1347.689, 2906.836, 3001.908, 3001.908	
CH_2	Cu-Ni-1	167.234, 269.135, 322.781, 435.518, 579.341, 666.582, 1285.554, 2872.344, 2910.766	
CH	Cu-Ni-1	397.919, 464.466, 617.442, 646.000, 662.297, 3046.711	
C_{surf}	Cu-Ni-1	452.316, 495.721, 715.536	
C_{sub-1}	Cu-Ni-1	549.827, 576.899, 704.197	
C_{sub-2}	Cu-Ni-1	596.153, 596.153,	

		651.499	
CH_3	Cu-Ni-2	210.454, 211.568, 335.586, 348.486, 463.841, 521.565, 1143.750, 1261.500, 1336.882, 2721.784, 2883.160, 2909.404	
CH_2	Cu-Ni-2	204.434, 286.545, 328.784, 439.364, 558.248, 669.587, 1284.197, 2871.880, 2908.049	
CH	Cu-Ni-2	390.217, 459.710, 615.219, 636.101, 673.553, 3044.787	
C_{surf}	Cu-Ni-2	456.712, 499.462, 735.526	
C_{sub-1}	Cu-Ni-2	548.682, 637.004, 680.486	
C_{sub-2}	Cu-Ni-2	564.321, 595.703, 699.301	
CH_3	Cu-Ni-3	166.259, 205.156, 275.822, 354.871, 433.926, 525.402, 1134.422, 1281.649, 1335.802, 2775.161, 2893.128, 2924.880	
CH_2	Cu-Ni-3	249.670, 292.333, 355.446, 487.169, 571.164, 669.054, 1329.825, 2732.693, 2959.198	
CH	Cu-Ni-3	385.765, 464.267, 592.411, 618.568, 663.712, 3041.693	
C_{surf}	Cu-Ni-3	464.385, 511.015, 728.083	
C_{sub-1}	Cu-Ni-3	533.296, 634.533,	

		673.969	
$C_{sub\text{-}2}$	Cu-Ni-3	568.958, 638,589, 695,693	

References

1 K. Kuchitsu and G. Graner, Structure of free polyatomic molecules : basic data, 1998, 214.

2 K. K. Irikura and D. J. Frurip, Computational Thermochemistry, 1998, **677**, https://doi.org/10.1021/BK-1998-0677.

3 Y. He, H. Wang, S. Jiang and Y. Mo, *Comput. Mater. Sci.*, 2019, **168**, 17–24, https://doi.org/10.1016/J.COMMATSCI.2019.05.046.

4 X. Pang, J. Yang, M. Pang and Y. Zhao, *J. Alloys Compd.*, 2020, **831**, 154747, https://doi.org/10.1016/j.jallcom.2020.154747.

5 K. Li, C. He, M. Jiao, Y. Wang and Z. Wu, *Carbon*, 2014, **74**, 255–265, https://doi.org/10.1016/J.CARBON.2014.03.030.

6 W. W. Pai, H. T. Jeng, C. –M. Cheng, C. –H. Lin, X. Xiao, A. Zhao, X. Zhang, G. Xu, X. Q. Shi, M. A. V. Hove, C. –S. Hsue and K. –D. Tsuei, *Phys. Rev. Lett.*, 2010, **104**, 036103, https://doi.org/10.1103/PhysRevLett.104.036103.

7 Y. –X. Wang and G. –C. Wang, *ACS Catal.*, 2019, **9**, 2261−2274, https://doi.org/10.1021/acscatal.8b04427.

8 K. Reuter and M. Scheffler, *Phys. Rev. B,* 2002, **65**, 1–11, https://doi.org/10.1103/PhysRevB.65.035406.

9 C. G. Van de Walle and J. Neugebauer, *Phys. Rev. Lett.*, 2002, **88**, 4, https://doi.org/10.1103/PhysRevLett.88.066103.

10 P. Li and Z. Li, *J. Phys. Chem. C*, 2020, **124**, 16233–16247, https://doi.org/10.1021/acs.jpcc.0c02040.

11 A. Mohsenzadeh, K. Bolton and T. Richards, *Surf. Sci.*, 2014, **627**, 1–10, 2014, https://doi.org/10.1016/j.susc.2014.04.006.

12 Y. A. Zhu, D. Chen, X. G. Zhou and W. K. Yuan, *Catal. Today*, 2009, **148**, 260–267, https://doi.org/10.1016/J.CATTOD.2009.08.022.

13 M. E. Jacox, J. Phys. Chem. Ref. Data, 2003, **32**, 1, https://doi.org/10.1063/1.1497629.

14 Y. Kangawa, T. Ito, A. Taguchi, K. Shiraishi and T. Ohachi, *Surf. Sci.*, 2001, **493**, 178–181, https://doi.org/10.1016/S0039-6028(01)01210-9.

15 Y. Kangawa, T. Akiyama, T. Ito, K. Shiraishi and T. Nakayama, *Materials*, 2013, **6**, 3309–3360 https://doi.org/10.3390/MA6083309